

Deep Reinforcement Learning based Robot Navigation in Dynamic Environments using Occupancy Values of Motion Primitives

Neşet Ünver Akmandor^{1*}, Hongyu Li^{2†}, Gary Lvov^{1‡}, Eric Dusel^{1§} and Taşkın Padır³

Abstract—This paper presents a Deep Reinforcement Learning based navigation approach in which we define the occupancy observations as heuristic evaluations of motion primitives, rather than using raw sensor data. Our method enables fast mapping of the occupancy data, generated by multi-sensor fusion, into trajectory values in 3D workspace. The computationally efficient trajectory evaluation allows dense sampling of the action space. We utilize our occupancy observations in different data structures to analyze their effects on both training process and navigation performance. We train and test our methodology on two different robots within challenging physics-based simulation environments including static and dynamic obstacles. We benchmark our occupancy representations with other conventional data structures from state-of-the-art methods. The trained navigation policies are also validated successfully with physical robots in dynamic environments. The results show that our method not only decreases the required training time but also improves the navigation performance as compared to other occupancy representations. The open-source implementation of our work and all related info are available at <https://github.com/RIVeR-Lab/tentabot>.

I. INTRODUCTION

Autonomous navigation in dynamic environments remains a challenging problem in robot motion planning [1], [2]. Although classical approaches such as graph-based [3], [4] and sampling-based [5], [6] methods can generate optimal paths, these techniques require prior map information while taking into account only static obstacles. This shortcoming limits their utility in real-world scenarios, such as autonomous driving within crowds [7], [8]. On the other hand, optimization-based methods [9], [10] and reactive algorithms [11]–[13] are capable of avoiding dynamic obstacles. However, these approaches are limited as they require pre-determined motion models of the moving obstacles.

In recent years, Deep Reinforcement Learning (DRL) based approaches have shown remarkable results in mobile robot navigation [14]–[19] in unknown environments. Through observing their environment via sensors, trained agents in these works are able to explore unknown areas while avoiding obstacles. Although their efficiency depends

on their training process, these data-driven approaches have two main advantages over classical methods. First, they gradually improve their performance during training by increasing the entropy of the defined state-action space. Second, they do not need an actual model of the environment to guide them to reach a successful policy. Despite their reported success, end-to-end learning methods require extensive training to achieve the desired navigation task [20], [21] due to large observation spaces. Without a model of their environment, these approaches try to estimate the necessary state values by interpreting high volumes of raw sensor data. To reduce the size of the input data, researchers mainly use Convolutional Neural Network (CNN) [22] and Variational Auto-Encoder (VAE) [21] architectures. However, these methods add extra training process on top of the navigation tasks.

While the assumption of having the environment model is impractical for navigation tasks, calculating the kinematic model of a robot is straightforward. Using that, one can filter the workspace information based on the task. To the best of our knowledge, no previous work utilizes the robot's kinematic model in 3D workspace in order to reduce the size of the required observation space using the DRL architecture.

A. Contribution

To improve the efficiency of the DRL methods for robot navigation in dynamic environments, our contributions in this paper include:

- Synthesizing computationally efficient trajectory occupancy values, considering the robot's kinematics model in 3D workspace. We present their structural variants as inputs to different neural networks in the DRL architecture and analyze their effects on navigation performance.
- Analyzing the performance of our occupancy representations by objectively comparing them with other state-of-the-art data structures within our presented framework. The policy of the robot is trained in challenging and various physics-based simulation environments.
- Validating our presented methods and navigation framework via simulation and real-world tests on two different mobile robots.
- Open-sourcing our work and results by providing our implementation and benchmark data in an code repository, which can be reached at <https://github.com/RIVeR-Lab/tentabot>.

*This research is supported by the National Science Foundation under Award Number 1928654.

¹Department of Electrical and Computer Engineering, Northeastern University, Boston, MA, 02115, USA *{akmandor.n}, ‡{lvov.g}, §{dusel.e}@northeastern.edu

²Khoury College of Computer Sciences, Northeastern University, Boston, MA, 02115, USA †li.hongyu1@northeastern.edu

³Institute for Experiential Robotics, Boston, MA, 02115, USA t.padir@northeastern.edu

II. RELATED WORK

In the literature of robot navigation, several methodologies are verified to be useful in the presence of moving obstacles. Given the trajectory estimation of dynamical objects, classical methods, such as graph-based [23] and optimization-based [24], [25], are able to find robust and collision free trajectories. While their mathematical guarantees make them reliable over data-driven methods, classical methods suffer from computational complexity when the condition space, i.e. the number of moving obstacles, is scaled up. Another drawback of these classical approaches is the assumption of having future trajectory information of dynamic obstacles. Although there are data driven methods [26], [27] that successfully predict human walking trajectories, they cannot be generalized for more complex motion models where the intentions of real-world agents can abruptly change.

Instead of assuming to know the agents' future trajectories, DRL based studies [15], [28]–[34] intrinsically estimate them by including the available obstacle data in their observation space. Considering the progress in pattern recognition and image processing, extracting the necessary information such as position, velocity, and each object's bounding box from the sensor data are more feasible than predicting obstacles' trajectories. Yet, the quality of the data extraction for each obstacle determines the success of the learned policy. Having a limited processing time, these works are similarly restrained by the number of obstacles. Although the aforementioned papers present dynamic obstacle avoidance in crowds (up-to 90 agents as in [32]), this can only be achieved by using the available obstacle trajectories within their simulation environment. In contrast, [28], [33], [34] estimate pedestrian velocities from the 2D range scan data and RGB images of their physical robot. Despite their results, there remains a huge feasibility gap between simulation and actual experiments.

To avoid dynamic obstacles without estimating trajectories or extracting current states, robots can be trained by supervised policies with imitation learning [35]. Ross et al. present in [36] a learning based Micro Aerial Vehicles (MAVs) controller which is trained with human expert data. At each time step, camera data are mapped to a set of features as the observation. Then, the reactive control policy is learned by the neural network to resemble the expert's performance. To bypass the tedious supervised data collection process, Pfeiffer et al. use a motion planner as their expert operator to train their network model in [16]. Their observation space includes raw data from the LiDAR sensor and 3D target information. One particular disadvantage of such methods is that the learned policy is limited by the supervised system's capabilities.

Without the aforementioned inputs (predicted obstacle trajectory, observable obstacle states, and expert policy),

another group of work [14], [20], [21], [37]–[45] employs only occupancy observations to determine optimal navigation policy with DRL. To manage the elevated complexity, the researchers focus on finding efficient representations and neural network (NN) modules to encapsulate the necessary information to achieve the navigation task. Table I summarizes most relevant approaches to our work by listing their observation data, NN architectures, and reinforcement learning methods.

TABLE I: List of observation data, NN architectures and RL methods in DRL based robot navigation literature.

Ref.	Data (*Processed, †Stacked)	NN Architecture	RL Method
[14]	depth image	2D.CNN+FC	DQN
[37]	laser scan, target, action	FC	DDPG,
[38]	laser scan [†] , target, action	1D.CNN+FC	DQN
[39]	laser scan [†] , target, action	1D.CNN+FC	PPO
[40]	laser scan*, action	FC	PPO
[20]	laser scan* [†] , waypoints	1D.CNN+FC, 2D.CNN+FC	PPO
[41]	laser scan, target, action	FC	TD3
[42]	laser scan, depth image, waypoints, action	{1D+2D}.CNN+FC	SAC
[21]	laser scan, target, action	VAE+LSTM+1D.CNN+FC, VAE+LSTM+2D.CNN+FC	PPO
[43]	laser scan, waypoints, target	1D.CNN+FC	SAC
[44]	laser scan* [†] , target* [†] , action [†]	2D.CNN+FC	PPO
[45]	laser scan, depth image, action [†]	{1D+2D}.CNN+FC	D3QN
Ours	laser scan* [†] , depth image* [†] , target, action	FC,1D.CNN+FC 2D.CNN+FC	PPO

III. APPROACH

A. Problem Definition and Navigation Framework

We define our problem as a Partially Observable Markov Decision Process (POMDP) [46] since neither geometric models of static obstacles nor the trajectory of mobile agents are known prior to the navigation. The POMDP model $M = (S, A, T, R, \Omega, O, \gamma)$ consists of state space S , action space A , state transition function T , reward function R , finite set of observations Ω , observation function O and discount factor $\gamma \in [0, 1)$. Given the current state $s \in S$ and the selected action $a \in A$, the state transition function $T(s'|s, a)$ calculates the probability of the next state $s' \in S$. As the actual state of the robot is assumed to be unavailable in POMDP formulation, it is estimated based on the observation function $O(o|s', a)$ where $o \in \Omega$. At each time step, the agent chooses an action based on the recent observations and receives an immediate reward $r = R(s, a)$ from the environment. The main aim of this formulation is to find the policy function $\Pi(a|s)$ that maximizes the cumulative discounted reward. Therefore, the reward function needs to be designed to lead the agent toward the goal state.

Our proposed framework is given in Fig. 1. Our task, robot and environment-specific observation space, action space and reward function are described in sections III-C, III-B and III-D respectively. The state estimation and the policy function are jointly estimated by the neural network whose architecture is defined in Section III-E.

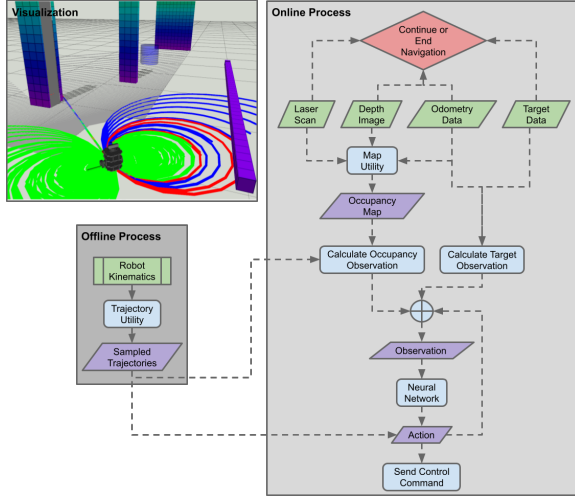


Fig. 1: Our navigation framework consists of two main stages: (1) In the Offline stage, trajectories are sampled using the robot’s kinematic model. A 3D grid structure, composed by voxels, is formed around the robot. The voxels are classified as either “Priority” or “Support” based on their proximity to the nearest sampling point. (2) During the Online stage, sensor data are mapped into classified voxels to enable the calculation of occupancy values for each trajectory. Using these observations as the input, the neural network outputs a discrete action. The online stage continues until a terminal state (goal or collision) is reached.

B. Action Space

Having linear $v \in [0, v^{max}]$ and angular $\omega \in [\omega^{min}, \omega^{max}]$ velocity limits of the robot’s controller, we uniformly sample both spaces by n^v and n^ω respectively. Providing initial states and discretized values of the action space as an input to the kinematic model, we form $n^k = n^v n^\omega$ trajectories. Hence, each trajectory j has one-to-one mapping to an action tuple (v_j, ω_j) . At each time step, the action index from the deep neural network output determines the velocity command.

Throughout this paper, we use 2D vector space to represent our actions $a = [v, \omega] \in \mathbb{R}^2$ since we perform our simulations on a differential drive robot controlled by linear v and angular ω velocity commands. However, our approach is readily applicable to 3D navigation and position-controlled systems, such as uninhabited aerial vehicles (UAVs) as well. In that case, the action space is defined as a 3D vector on the selected trajectory as in [47], [48].

C. Observation Space

Instead of including raw sensor information, such as laser scan as in [16], [21], [33], [37]–[39], [41]–[43], [45] or depth image as in [14], [31], [42], [45], [49], our observations utilize the occupancy information of the pre-sampled trajectories. To efficiently evaluate these trajectory values at each time step, the framework in [47],

[48] is adopted in our DRL based architecture. The 3D grid structure, formed by voxels, is centered at the robot’s frame R and initialized prior to navigation. We sample each trajectory j by n^{T_j} points ${}^R p_i = (x, y, z)$ and keep them in a set $T_j = \{{}^R p_i \mid i = 1, \dots, n^{T_j}\}$. Each voxel is defined as $\psi_k = (u_k, \beta_k, m_k, c_k)$, where u_k is the index that points out the k^{th} voxel position in the linearized array A_p which keeps coordinate positions of voxel centers. β_k is the user-defined weight for the corresponding voxel. m_k is the index of the closest sampling point on the trajectory to the k^{th} voxel. c_k indicates whether it is a Priority ($c = 1$) or Support ($c = 0$) voxel. The set of “Support” $S_j^\psi = \{\psi_k \mid k = 1, \dots, n^{S_j^\psi}, \tau^{P^\psi} < \|A_p(u_k) - T_{m_k}\| < \tau^{S^\psi}\}$ and “Priority” $P_j^\psi = \{\psi_k \mid k = 1, \dots, n^{P_j^\psi}, \|A_p(u_k) - T_{m_k}\| < \tau^{P^\psi}\}$ voxels inside the robot-centered 3D grid are extracted based on the user-defined thresholds τ^{S^ψ} and τ^{P^ψ} respectively.

Inspired by their formulation of two heuristic functions, which are “Clearance” and “Nearby Clutter”, we define our distinct occupancy function H^{occ} to represent both information as a single value. We define H^{occ} , as shown in Eq. 1, using similar notations in [48]. For each sampling point i in trajectory j , sum of voxel weights W_j is calculated by Eq. 2. At each time step, linearized array A_σ which consists of occupancy values inside the 3D grid are updated by the recent sensor data. The crash index u^{crash} is determined by the first occupied Priority voxel along the trajectory. Having A_σ and u^{crash} for each trajectory j , the weighted sum of voxel weights W_j^{scaled} is calculated by Eq. 3. Then, the occupancy value H_j^{occ} is obtained by W_j^{scaled} divided by the multiplication of W_j with the maximum occupancy value of a voxel σ^{max} . By definition, $H_j^{occ} \in [0, 1]$.

$$H_j^{occ} = \frac{W_j^{scaled}}{\sigma^{max} W_j} \quad (1)$$

$$W_j = \sum_{k=1}^{n^{S_j^\psi \cup P_j^\psi}} \beta_k, \quad (2)$$

$$W_j^{scaled} = \sum_{i=1}^{n^{S_j^\psi \cup P_j^\psi}} \alpha_{m_k} \beta_k, \quad (3)$$

where $\psi_k \in S_j^\psi \cup P_j^\psi$,

$$\text{and } \alpha_{m_k} = \begin{cases} A_\sigma(m_k) & \text{if } m_k < u^{crash} \\ \sigma^{max} & \text{else.} \end{cases}$$

Similar to [21], [37]–[39], [41], we include the target data $o^{target} = [d^{target}, \theta^{target}] \in \mathbb{R}^2$ and previous action $o^{action} = [v^{pre}, \omega^{pre}] \in \mathbb{R}^2$ in our observation space. The first field of the target data $d^{target} \in \mathbb{R}^+$ is defined as the Euclidean distance between the robot and the target. The second field is defined as the yaw angle $\theta^{target} \in [-\pi, \pi]$ to the target with respect to robot’s frame R .

To learn the dynamic characteristics of obstacles, analogous to [20], [38], [39], [44], we stack occupancy data from n^{stack} previous time steps as shown in Fig. 2. Since merely milliseconds pass between successive steps, we observe better results when we skip n^{skip} time steps when stacking the data to add into the observation space. The structure of the stacking depends on the NN architecture that we input our observations.

To utilize the fully connected (FC) layers as on the left in Fig. 3, we obtain our occupancy observations by concatenating one after another as in $o^{occ-1D} = [H_{1t}^{occ}, \dots, H_{n^k t}^{occ}, H_{1(t-n^{skip})}^{occ}, \dots, H_{n^k(t-n^{skip}n^{stack})}^{occ}] \in \mathbb{R}^{n^k n^{stack}}$. We consider the occupancy observation at each time step $o^{occ-C1D} = [H_1^{occ}, \dots, H_{n^k}] \in \mathbb{R}^{n^k}$ for the input to each channel in 1D-CNN architecture. Therefore for n^{stack} time steps, we have n^{stack} channels of data where each row belongs to a particular time step. For the input of 2D-CNN network, we present our occupancy data in a 2D array structure. Different from the 1D-CNN case, we form each column to represent the data at each time step. Therefore, the time stack of data concatenated in the row direction and the observation space becomes $o^{occ-2D} \in \mathbb{R}^{n^k \times n^{stack}}$.

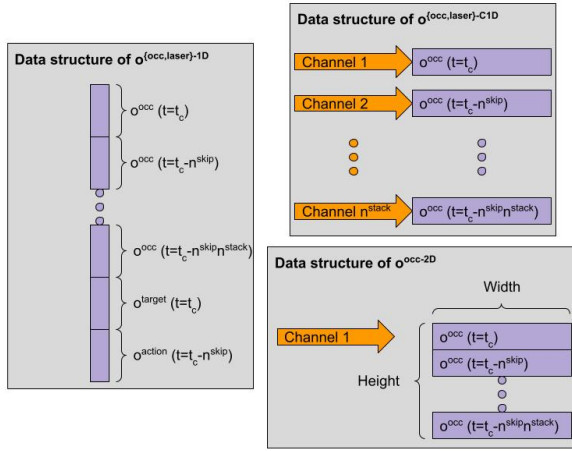


Fig. 2: Different structures of the observation data are generated by either laser range or trajectory occupancy values. Left: Data from different time steps are concatenated into a 1D array. Right-Top: For each time step, 1D array of data are passed into a channel. Right-Bottom: Each row of the 2D array structure is formed by the data at its corresponding time step. The height shows the number of stacked data from previous time steps.

D. Reward Function

We design our reward function as in Eq. 4 to supervise the robot to reach the goal and avoid collision with obstacles. We set a positive reward μ^{goal} when the robot reaches the goal. If the episode ends by either passing a threshold τ^{fail} value of a distance to the closest obstacle d_t^{obs} or reaching the maximum number of steps $n^{max.ep.ts}$ per episode, we

penalize it by a negative reward μ^{fail} . To reduce the training time that the robot might inefficiently spend to explore its state space, we define a step reward function μ_t^{step} to evaluate the states other than the end cases.

$$Reward = \begin{cases} \mu^{goal} & \text{if } d_t^{target} < \tau^{target} \\ \mu^{fail} & \text{else if } n_t > n^{max.ep.ts} \text{ or } d_t^{obs} < \tau^{fail} \\ \mu_t^{step} = \mu_t^{target} + \mu_t^{step-pen} & \text{else} \end{cases} \quad (4)$$

$$\text{where } \mu_t^{target} = \alpha^{target} (d_{t-\Delta t}^{target} - d_t^{target}) \quad (5)$$

$$\mu_t^{step-pen} = \frac{\alpha^{step-pen}}{n^{max.ep.ts}} \quad (6)$$

The first part of the step function μ_t^{target} is calculated by taking the difference between current and previous time steps' target distance and multiplying it with the user-defined scalar α^{target} to adjust the reward/penalty weight on the navigation. The target distance is calculated with respect to the robot's frame R . Based on the sign of the distance difference, the function either penalizes or rewards the current state. The second part of the step function $\mu_t^{step-pen}$ penalizes the robot for not reaching the goal. The penalty value $\mu_t^{step-pen}$ is fixed for each time and determined by the user-defined scalar $\alpha^{step-pen}$ and $n^{max.ep.ts}$ as in Eq. 6. Although the robot may tend to get stuck at local minima because of the greedy evaluations of our reward design, including previous action in observations helps robot to escape from dead spots by forcing it to choose different actions.

E. Neural Network Architectures

To analyze the effect of the input structure of our trajectory value observations on navigation performance, we train the robot using three different neural network architectures as shown in Fig. 3. The left side of Fig. 3 displays the fully connected (FC) layers which take the occupancy, either o^{occ-1D} or $o^{laser-1D}$, target o^{target} and action o^{action} observation inputs. We concatenate these three observations into a 1D array and feed it into the first layer of the FC network. The output of the network is mapped into one of the discrete actions defined in III-B. We also implement two different CNN networks both of which consist of 3 CNN layers followed by 2 FC layers as shown in the right side of Fig. 3. The only difference between both networks is the input structure of the observations as defined in Section III-C and visualized in Fig. 2.

F. Implementation Details

The core implementation of our work is built on the framework presented in [47], [48], which is developed in ROS architecture. We utilize that coding base to construct the necessary structures, such as 3D grid, voxels and heuristic functions, generate pre-sampled trajectories, and map the occupancy data coming from the sensors (RGB-D camera and 2D LiDAR). The Gazebo simulator is used to form physical environments, simulate and control realistic robots, such as Turtlebot3 and Hello Robot's Stretch. We create the dynamic obstacles as groups of walking

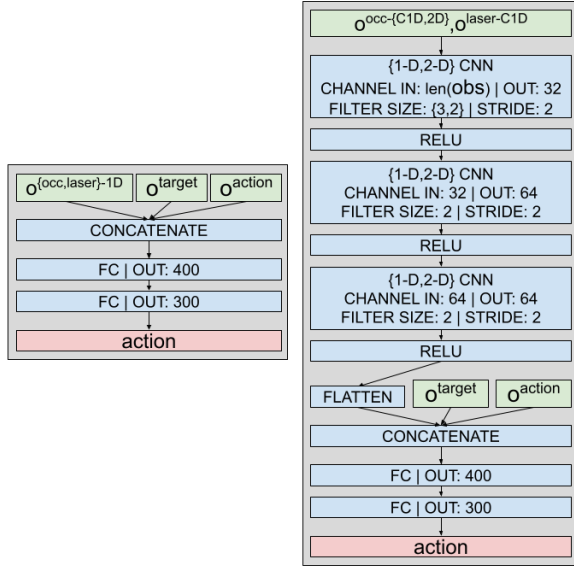


Fig. 3: Neural network architectures where the observation inputs are shown in green, network layers in blue and action output in red. Left: 2 FC layers. The observations o^{occ-1D} , $o^{laser-1D}$ are concatenated with target o^{target} and action o^{action} observations before going into FC layers. Right: 3-layer CNN followed by 2 FC layers. The occupancy observations o^{occ} , o^{laser} are fed into either 1D or 2D CNN depending on their data structures. The target o^{target} and action o^{action} observations are concatenated with the output of the CNN and then input into the FC layers.

pedestrians using the implementation of the work in [50]. We also use Gym [51], which is an open-source Python library for developing and benchmarking reinforcement learning algorithms. To construct a Gym environment within the ROS architecture, we utilize the ROS package in [52].

We use Proximal Policy Optimization (PPO) [53] to train our robot for the navigation task within dynamic environments. PPO is a policy gradient method which is suitable for both continuous and discrete action spaces. Notably, it provides stability by determining the maximum step size for the exploration, so that the deviation between the policy iterations is bounded by a trust region. We employ the Stable-Baselines3 [54] implementation of PPO, where they provide useful tools for customizing neural network architecture and monitoring the training process.

IV. RESULTS

A. Training

To train our robot in simulations, we create five different environments in Gazebo as shown in Fig. 4. The environments labeled as $T0(S)$ and $T1(S)$ contain only static obstacles such that $T0(S)$ has two cubic (1 m diameter) objects and $T1(S)$ has more distinct objects. On the other hand, $T0(D)$ and $T1(D)$ labeled maps include only dynamic objects in the shape of rectangular cuboids (width: 0.2 m,

length: 0.2 m, height: 1 m). Similar to static maps, the number of obstacles in $T1(D)$ is higher than $T0(D)$ with 13 dynamic obstacles as opposed to 2. $T2(D)$ includes both static and dynamic obstacles. The area of $T0(S)$ and $T0(D)$ are $6 \times 4 \text{ m}^2$ while $T0(S)$, $T1(S)$ and $T2(D)$ are $12 \times 10 \text{ m}^2$.

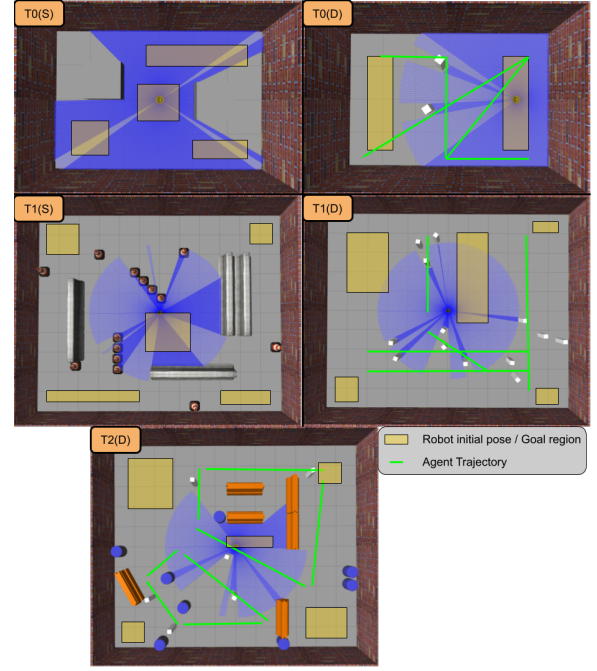


Fig. 4: Training environments: $T0(S)$ and $T1(S)$ contain only static objects. $T0(D)$ and $T1(D)$ labeled maps include only dynamic objects in the shape of rectangular cuboids. $T2(D)$ includes both static and dynamic obstacles. Robot and goal positions are randomized inside of the yellow areas.

At the beginning of each training episode, the robot is initialized at a random position inside the yellow areas of the respective map in Fig. 4. The goal position is also randomly selected from these areas, without coinciding with the initial area of the robot. Similar to [41], we use hierarchical training methodology starting from $T0(S)$, which has a small area and only contains static obstacles. Whenever we observe a convergence in cumulative rewards, we switch training in a more complex map in the order of $T1(S)$, $T0(D)$, $T1(D)$ and $T2(D)$. During our experiments, we found that the hierarchical process can remarkably improve the convergence rate compared to training only within a single complex map.

Our training benchmark includes seven different approaches which differ from each other by the occupancy data structures (raw laser scan, image representation [20], polar representation [21], our occupancy representation which is labeled as Tentabot) and neural network architectures (FC, 1DCNN_FC, 2DCNN_FC). To speed up the computation without effecting the performance for laser_FC and laser_1DCNN_FC, we reduce the total number of laser scans from 360 to 90 by filtering them equidistantly. For the fairness of comparisons as having similar number of

occupancy values in our variants, we linearly sample lateral and angular velocities by 5 and 21 respectively. That leads to 105 trajectories with their occupancy values. Since our occupancy values are defined in the range of $[0, 1]$, we also normalize the laser scan data. To benchmark our proposed value function, we use two different representations of the laser data: the 2D image representation from [20] labeled as `laser_image` and the polar image representation from [21] labeled as `laser_rings`.

We train all approaches using the aforementioned hierarchical methodology, where each training environment is run for 200k time steps. Since the cumulative rewards of `laser_image` and `laser_rings` could not reach positive values, even after 200k training steps in the first map $T0(S)$, we do not proceed with their training. Although the training performance of `Tentabot_2DCNN_FC` is as successful as `Tentabot_1DCNN_FC`, we also do not continue its training after it clearly outperforms its image counterparts, to reserve our limited computational resources for other comparisons. The overall training results in Fig. 5 show that higher cumulative rewards are achieved when the observations include our proposed occupancy value o^{occ} over o^{laser} . Although the `laser_1DCNN_FC` converges faster than `Tentabot_1DCNN_FC`, they both gain competitive rewards during the training process. Similarly, there is no clear winner between `laser_FC` and `Tentabot_FC`. Here, we should point out that our representation has an important disadvantage against its laser counterparts. Although we use same network structures for each comparison, our occupancy representation has 75 more values, as we stack 5 previous observations, which causes less learning within the same amount of time. As a future work, we will address this issue by optimizing hyper-parameters, such as number of layers and number of neurons in these layers, of the neural network for each of these data structures.

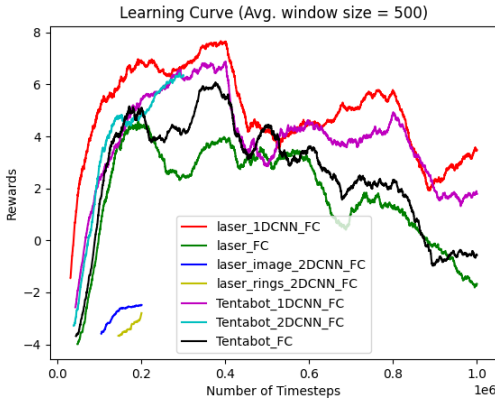


Fig. 5: Cumulative learning curve of the training data.

B. Testing

To compare the navigation policies trained by the different approaches, we perform simulation tests in five environments

as shown in Fig. 6. We create these environments with distinct static obstacles and map features different from the training maps to demonstrate that our models are not overfitting. The testing environments include overtaking an agent moving towards the goal (Fig 7a), overtaking agents moving towards the robot (Fig 7b), avoiding agents which cross in front of the robot (Fig 7c), crossing a complex static environment (Fig 7d), and crossing complex static environment with random dynamic agents (Fig 7e).

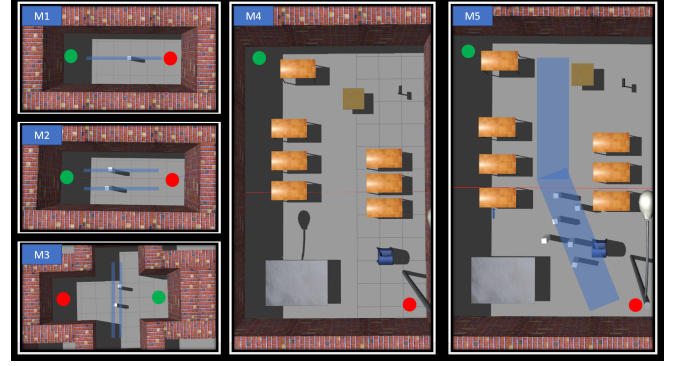


Fig. 6: Testing environments. The blue areas represent agent trajectories. The green dots represent initial point, and the red dots represent the goals.

Based on the training results in Fig. 5, we perform navigation tests using four successfully trained policies; `laser_FC`, `laser_1DCNN_FC`, `Tentabot_FC`, `Tentabot_1DCNN_FC`, and two reactive planners; `Tentabot_Heuristic` [47] and `Timed Elastic Band (TEB)` [55]. We compare their performance in terms of navigation success rate (Fig 7). To test the robustness of each policy, we perform the same task ten times and calculate their mean values. The testing results show that the policies trained with our approach (`Tentabot_FC`, `Tentabot_1DCNN_FC`, and `Tentabot_2DCNN_FC`) navigate with higher success rate and reach the goal faster than the `laser_FC`, which utilizes normalized laser data. Moreover, `Tentabot_1DCNN_FC` outperforms all other approaches in the crossing environment (Fig 7c), and matches with `TEB` in the complex static and dynamic environment (Fig 7e). Even though `laser_1DCNN_FC` performs well in the training and the first three testing environments (Fig 7a, Fig 7b, Fig 7c) where obstacles are structured, it performs poorly when the map consists of novel obstacles as in (Fig 7d, 7e). Our approach demonstrates greater performance in novel environments compared to the laser-based counterparts due to its embedded occupancy representation of the 3D workspace.

C. Real-robot Testing

We use the trained `Tentabot_FC` policy on the Stretch from Hello Robot (Fig. 8a) which is equipped with a Slamtex RPLiDAR A1, Intel RealSense D435i RGB-D Camera, and an onboard computer (Intel i5-8259U with 16GB RAM). We publish various goals in multiple environment settings (no obstacles, static obstacles, dynamic obstacles, and crowd) to test the performance of our work. In real world experiments,

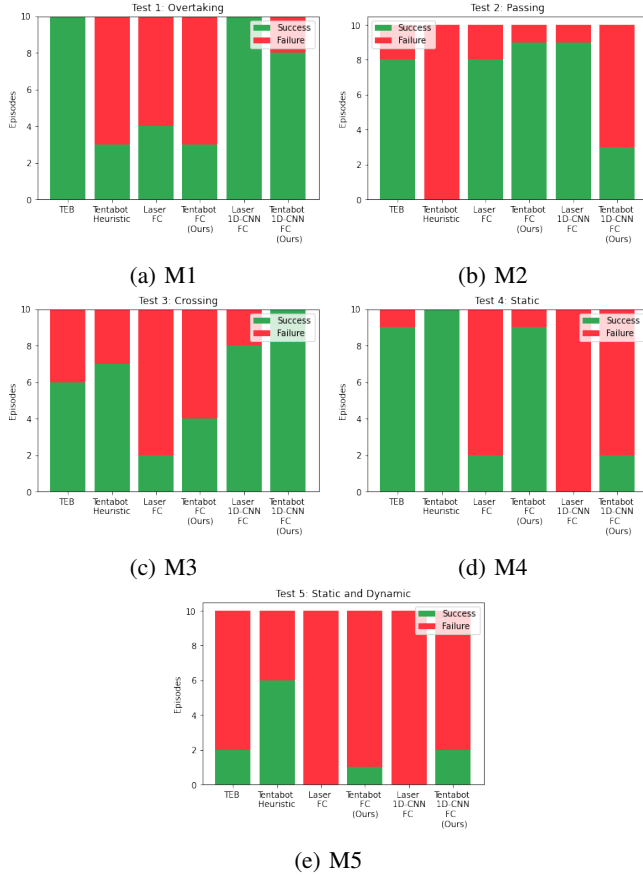


Fig. 7: Testing results of different navigation approaches in 5 distinct environments. Approaches from left to right: TEB, Tentabot_Heuristic, laser_FC, Tentabot_FC, laser_1DCNN_FC, Tentabot_1DCNN_FC. Each of the DRL based approaches is trained one million time steps which takes around 50 hours.

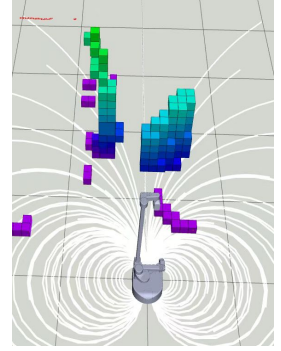
our robot reaches the goal every time, even it has some physical contacts with dynamic agents but without colliding any static obstacle. Although we sometime observe that the robot circles around the goal, we infer that is due to the lack of parameter tuning in our reward function.

V. CONCLUSIONS

In this paper, we introduce a DRL based robot navigation approach which uses occupancy values of pre-sampled trajectories as a part of the observation space. We present variants of this representation by utilizing different neural network architectures. To verify our approach, we implement our open-source work in a physics-based simulator. We train and test our policy in various simulation environments. We benchmark our approach against other conventional occupancy data. The results show that our method not only decreases the required training time, but also increases the success rate of the navigation. As a future work, we will estimate our reward function as a neural network trained with an expert data in order to adapt our approach in more challenging real-world applications.



(a) Real world scene



(b) Visualization in RViz

Fig. 8: (a) We test our navigation approach in real world scenarios where static obstacles and dynamic agents are involved. (b) Our software runs in the robot's onboard computer where the real-time data, such as pre-sampled trajectories and occupied voxels, can be visualized.

REFERENCES

- [1] J. Cheng, H. Cheng, M. Q.-H. Meng, and H. Zhang, "Autonomous navigation by mobile robots in human environments: A survey," in *2018 IEEE International Conference on Robotics and Biomimetics (ROBIO)*. IEEE, 2018, pp. 1981–1986.
- [2] K. Cai, C. Wang, J. Cheng, C. W. De Silva, and M. Q.-H. Meng, "Mobile robot path planning in dynamic environments: a survey," *arXiv preprint arXiv:2006.14195*, 2020.
- [3] E. W. Dijkstra *et al.*, "A note on two problems in connexion with graphs," *Numerische mathematik*, vol. 1, no. 1, pp. 269–271, 1959.
- [4] P. E. Hart, N. J. Nilsson, and B. Raphael, "A formal basis for the heuristic determination of minimum cost paths," *IEEE Transactions on Systems Science and Cybernetics*, vol. 4, no. 2, pp. 100–107, 1968.
- [5] S. M. LaValle *et al.*, "Rapidly-exploring random trees: A new tool for path planning," 1998.
- [6] S. Karaman and E. Frazzoli, "Sampling-based algorithms for optimal motion planning," *The International Journal of Robotics Research*, vol. 30, no. 7, pp. 846–894, 2011.
- [7] H. Bai, S. Cai, N. Ye, D. Hsu, and W. S. Lee, "Intention-aware online pomdp planning for autonomous driving in a crowd," in *2015 IEEE International Conference on Robotics and Automation (ICRA)*. IEEE, 2015, pp. 454–460.
- [8] Y. Luo, P. Cai, A. Bera, D. Hsu, W. S. Lee, and D. Manocha, "Porca: Modeling and planning for autonomous driving among many pedestrians," *IEEE Robotics and Automation Letters*, vol. 3, no. 4, pp. 3418–3425, 2018.
- [9] X. Liu, H. Chen, C. Wang, F. Hu, and X. Yang, "Mpc control and path planning of omni-directional mobile robot with potential field method," in *International Conference on Intelligent Robotics and Applications*. Springer, 2018, pp. 170–181.
- [10] A. S. Lafmejani and S. Berman, "Nonlinear mpc for collision-free and deadlock-free navigation of multiple nonholonomic mobile robots," *Robotics and Autonomous Systems*, vol. 141, p. 103774, 2021.
- [11] D. Fox, W. Burgard, and S. Thrun, "The dynamic window approach to collision avoidance," *IEEE Robotics & Automation Magazine*, vol. 4, no. 1, pp. 23–33, 1997.
- [12] S. Quinlan and O. Khatib, "Elastic bands: Connecting path planning and control," in *[1993] Proceedings IEEE International Conference on Robotics and Automation*. IEEE, 1993, pp. 802–807.
- [13] I. Ulrich and J. Borenstein, "Vfh: local obstacle avoidance with look-ahead verification, robotics and automation, 2000," in *Proceedings. ICRA'00. IEEE International Conference on*, vol. 3, 2000.
- [14] L. Tai and M. Liu, "A robot exploration strategy based on q-learning network," in *2016 IEEE International Conference on Real-time Computing and Robotics (RCAR)*. IEEE, 2016, pp. 57–62.
- [15] Y. F. Chen, M. Liu, M. Everett, and J. P. How, "Decentralized non-communicating multiagent collision avoidance with deep reinforce-

- ment learning,” in *2017 IEEE International Conference on Robotics and Automation (ICRA)*. IEEE, 2017, pp. 285–292.
- [16] M. Pfeiffer, M. Schaeuble, J. Nieto, R. Siegwart, and C. Cadena, “From perception to decision: A data-driven approach to end-to-end motion planning for autonomous ground robots,” in *2017 IEEE International Conference on Robotics and Automation (ICRA)*. IEEE, 2017, pp. 1527–1533.
 - [17] C. Yan, X. Xiang, and C. Wang, “Towards real-time path planning through deep reinforcement learning for a uav in dynamic environments,” *Journal of Intelligent & Robotic Systems*, vol. 98, no. 2, pp. 297–309, 2020.
 - [18] O. Doukhi and D.-J. Lee, “Deep reinforcement learning for end-to-end local motion planning of autonomous aerial robots in unknown outdoor environments: Real-time flight experiments,” *Sensors*, vol. 21, no. 7, p. 2534, 2021.
 - [19] C. Xu, C. Amato, and L. L. Wong, “Hierarchical robot navigation in novel environments using rough 2-d maps,” *arXiv preprint arXiv:2106.03665*, 2021.
 - [20] R. Guldenring, M. Görner, N. Hendrich, N. J. Jacobsen, and J. Zhang, “Learning local planners for human-aware navigation in indoor environments,” in *2020 IEEE/RSJ International Conference on Intelligent Robots and Systems (IROS)*. IEEE, 2020, pp. 6053–6060.
 - [21] D. Dugas, J. Nieto, R. Siegwart, and J. J. Chung, “Navrep: Unsupervised representations for reinforcement learning of robot navigation in dynamic human environments,” *arXiv preprint arXiv:2012.04406*, 2020.
 - [22] N. Botteghi, K. Alaa, M. Poel, B. Sirmacek, C. Brune, A. Mersha, and S. Stramigioli, “Low dimensional state representation learning with robotics priors in continuous action spaces,” in *2021 IEEE/RSJ International Conference on Intelligent Robots and Systems (IROS)*. IEEE, 2021, pp. 190–197.
 - [23] T. Fraichard and A. Scheuer, “Car-like robots and moving obstacles,” in *Proceedings of the 1994 IEEE International Conference on Robotics and Automation*. IEEE, 1994, pp. 64–69.
 - [24] T. Schoels, P. Rutquist, L. Palmieri, A. Zanelli, K. O. Arras, and M. Diehl, “Ciao*: Mpc-based safe motion planning in predictable dynamic environments,” *IFAC-PapersOnLine*, vol. 53, no. 2, pp. 6555–6562, 2020.
 - [25] B. Lindqvist, S. S. Mansouri, A.-a. Agha-mohammadi, and G. Nikolakopoulos, “Nonlinear mpc for collision avoidance and control of uavs with dynamic obstacles,” *IEEE Robotics and Automation Letters*, vol. 5, no. 4, pp. 6001–6008, 2020.
 - [26] A. Alahi, K. Goel, V. Ramanathan, A. Robicquet, L. Fei-Fei, and S. Savarese, “Social lstm: Human trajectory prediction in crowded spaces,” in *Proceedings of the IEEE Conference on Computer Vision and Pattern Recognition*, 2016, pp. 961–971.
 - [27] N. Shafiee, T. Padi, and E. Elhamifar, “Introvert: Human trajectory prediction via conditional 3d attention,” in *Proceedings of the IEEE/CVF Conference on Computer Vision and Pattern Recognition*, 2021, pp. 16815–16825.
 - [28] Y. F. Chen, M. Everett, M. Liu, and J. P. How, “Socially aware motion planning with deep reinforcement learning,” in *2017 IEEE/RSJ International Conference on Intelligent Robots and Systems (IROS)*. IEEE, 2017, pp. 1343–1350.
 - [29] M. Everett, Y. F. Chen, and J. P. How, “Motion planning among dynamic, decision-making agents with deep reinforcement learning,” in *2018 IEEE/RSJ International Conference on Intelligent Robots and Systems (IROS)*. IEEE, 2018, pp. 3052–3059.
 - [30] C. Chen, Y. Liu, S. Kreiss, and A. Alahi, “Crowd-robot interaction: Crowd-aware robot navigation with attention-based deep reinforcement learning,” in *2019 International Conference on Robotics and Automation (ICRA)*. IEEE, 2019, pp. 6015–6022.
 - [31] A. J. Sathiamoorthy, J. Liang, U. Patel, T. Guan, R. Chandra, and D. Manocha, “Densecavoid: Real-time navigation in dense crowds using anticipatory behaviors,” in *2020 IEEE International Conference on Robotics and Automation (ICRA)*. IEEE, 2020, pp. 11 345–11 352.
 - [32] Q. Tan, T. Fan, J. Pan, and D. Manocha, “Deepmnavigate: Deep reinforced multi-robot navigation unifying local & global collision avoidance,” in *2020 IEEE/RSJ International Conference on Intelligent Robots and Systems (IROS)*. IEEE, 2020, pp. 6952–6959.
 - [33] L. Kästner, C. Marx, and J. Lambrecht, “Deep-reinforcement-learning-based semantic navigation of mobile robots in dynamic environments,” in *2020 IEEE 16th International Conference on Automation Science and Engineering (CASE)*. IEEE, 2020, pp. 1110–1115.
 - [34] M. Everett, Y. F. Chen, and J. P. How, “Collision avoidance in pedestrian-rich environments with deep reinforcement learning,” *IEEE Access*, vol. 9, pp. 10 357–10 377, 2021.
 - [35] A. Hussein, M. M. Gaber, E. Elyan, and C. Jayne, “Imitation learning: A survey of learning methods,” *ACM Computing Surveys (CSUR)*, vol. 50, no. 2, pp. 1–35, 2017.
 - [36] S. Ross, N. Melik-Barkhudarov, K. S. Shankar, A. Wendel, D. Dey, J. A. Bagnell, and M. Hebert, “Learning monocular reactive uav control in cluttered natural environments,” in *2013 IEEE International Conference on Robotics and Automation*. IEEE, 2013, pp. 1765–1772.
 - [37] L. Tai, G. Paolo, and M. Liu, “Virtual-to-real deep reinforcement learning: Continuous control of mobile robots for mapless navigation,” in *2017 IEEE/RSJ International Conference on Intelligent Robots and Systems (IROS)*. IEEE, 2017, pp. 31–36.
 - [38] L. Xie, S. Wang, S. Rosa, A. Markham, and N. Trigoni, “Learning with training wheels: speeding up training with a simple controller for deep reinforcement learning,” in *2018 IEEE International Conference on Robotics and Automation (ICRA)*. IEEE, 2018, pp. 6276–6283.
 - [39] P. Long, T. Fan, X. Liao, W. Liu, H. Zhang, and J. Pan, “Towards optimally decentralized multi-robot collision avoidance via deep reinforcement learning,” in *2018 IEEE International Conference on Robotics and Automation (ICRA)*. IEEE, 2018, pp. 6252–6259.
 - [40] J. Zeng, R. Ju, L. Qin, Y. Hu, Q. Yin, and C. Hu, “Navigation in unknown dynamic environments based on deep reinforcement learning,” *Sensors*, vol. 19, no. 18, p. 3837, 2019.
 - [41] J. Gao, W. Ye, J. Guo, and Z. Li, “Deep reinforcement learning for indoor mobile robot path planning,” *Sensors*, vol. 20, no. 19, p. 5493, 2020.
 - [42] Q. Liu, Y. Li, and L. Liu, “A 3d simulation environment and navigation approach for robot navigation via deep reinforcement learning in dense pedestrian environment,” in *2020 IEEE 16th International Conference on Automation Science and Engineering (CASE)*. IEEE, 2020, pp. 1514–1519.
 - [43] C. Pérez-D’Arpino, C. Liu, P. Goebel, R. Martín-Martín, and S. Savarese, “Robot navigation in constrained pedestrian environments using reinforcement learning,” *arXiv preprint arXiv:2010.08600*, 2020.
 - [44] U. Patel, N. K. S. Kumar, A. J. Sathiamoorthy, and D. Manocha, “Dwa-rl: Dynamically feasible deep reinforcement learning policy for robot navigation among mobile obstacles,” in *2021 IEEE International Conference on Robotics and Automation (ICRA)*. IEEE, 2021.
 - [45] H. Song, A. Li, T. Wang, and M. Wang, “Multimodal deep reinforcement learning with auxiliary task for obstacle avoidance of indoor mobile robot,” *Sensors*, vol. 21, no. 4, p. 1363, 2021.
 - [46] L. P. Kaelbling, M. L. Littman, and A. R. Cassandra, “Planning and acting in partially observable stochastic domains,” *Artificial intelligence*, vol. 101, no. 1-2, pp. 99–134, 1998.
 - [47] N. Ü. Akmandor and T. Padi, “A 3d reactive navigation algorithm for mobile robots by using tentacle-based sampling,” in *2020 Fourth IEEE International Conference on Robotic Computing (IRC)*. IEEE, 2020, pp. 9–16.
 - [48] N. Ü. Akmandor and T. Padi, “Reactive navigation framework for mobile robots by heuristically evaluated pre-sampled trajectories,” *International Journal of Robotic Computing*, vol. 3, no. 1, pp. 47–68, 2021.
 - [49] L. Tai, J. Zhang, M. Liu, and W. Burgard, “Socially compliant navigation through raw depth inputs with generative adversarial imitation learning,” in *2018 IEEE International Conference on Robotics and Automation (ICRA)*. IEEE, 2018, pp. 1111–1117.
 - [50] B. Okal and K. O. Arras, “Towards group-level social activity recognition for mobile robots,” in *IROS Assistance and Service Robotics in a Human Environments Workshop*, 2014.
 - [51] G. Brockman, V. Cheung, L. Pettersson, J. Schneider, J. Schulman, J. Tang, and W. Zaremba, “Openai gym,” 2016.
 - [52] M. A. R. Alberto Ezquerro and R. Tellez, “Openai-ros,” <http://wiki.ros.org/openai-ros>.
 - [53] J. Schulman, F. Wolski, P. Dhariwal, A. Radford, and O. Klimov, “Proximal policy optimization algorithms,” *arXiv preprint arXiv:1707.06347*, 2017.
 - [54] A. Raffin, A. Hill, M. Ernestus, A. Gleave, A. Kanervisto, and N. Dormann, “Stable baselines3,” <https://github.com/DLR-RM/stable-baselines3>, 2019.
 - [55] C. Rösmann, W. Feiten, T. Wösch, F. Hoffmann, and T. Bertram, “Efficient trajectory optimization using a sparse model,” in *2013 European Conference on Mobile Robots*, 2013, pp. 138–143.